Polarization modulation for fluorescence emission difference microscopy

Nan Wang[1,2] **and Takayoshi Kobayashi**[1,2,3,4,*]

[1]*Advanced Ultrafast Laser Research Center, University of Electro-Communications, 1-5-1 Chofugaoka, Chofu, Tokyo 182-8585, Japan*
[2]*JST, CREST, 5 Sanbancho, Chiyoda-ku, Tokyo 102-0075, Japan*
[3]*Advanced Ultrafast Laser Research Center, Department of Electrophysics, National Chiao-Tung University, 1001 Ta Hsinchu Rd., Hsinchu 300, Taiwan*
[4]*Insitute of Laser Engineering, Osaka University, 2-6 Yamada-oka, Suita, Osaka 565-0971, Japan*

[*]*kobayashi@ils.uec.ac.jp*

Abstract: Effects of the polarization on subtracted images in fluorescence emission difference microscopy are numerically investigated based on vector beam diffraction theory and alteration of Jones matrices. Parameters of resolution, signal loss, and amplitude of negative sidebands after subtraction are discussed along with the polarization of excitation beams and sample sizes. The effects of polarization on the ellipticity and subtraction threshold are also given.

OCIS codes: (100.6640) Image analysis; (000.3860) Mathematical methods in physics; (180.2520) Fluorescence microscopy; (260.5430) Polarization.

References and links

1. S. W. Hell and J. Wichmann, "Breaking the diffraction resolution limit by stimulated emission: stimulated-emission-depletion fluorescence microscopy," Opt. Lett. **19**(11), 780–782 (1994).
2. M. G. L. Gustafsson, "Surpassing the lateral resolution limit by a factor of two using structured illumination microscopy," J. Microscopy **198**, 82–87 (2000).
3. E. Betzig, G. H. Patterson, R. Sougrat, O. W. Lindwasser, S. Olenych, J. S. Bonifacino, M. W. Davidson, J. L. Schwartz, and H. F. Hess, "Imaging intracellular fluorescent proteins at nanometer resolution," Science **313**, 1642–1645 (2006).
4. M. J. Rust, M. Bates, and X. W. Zhuang, "Sub-diffraction-limit imaging by stochastic optical reconstruction microscopy (STORM)," Nat. Meth. **3**, 793–796 (2006).
5. M. P. Gordon, T. Ha, and P. R. Selvin, "Single-molecule high-resolution imaging with photobleaching," P. Natl. Acad. Sci. USA **101**(17), 6462–6465 (2004).
6. A. Sharonov and R. M. Hochstrasser, "Wide-field sub-diffraction imaging by accumulated binding of diffusing probes," P. Natl. Acad. Sci. USA **103**(50), 18911–18916 (2006).
7. K. Fujita, M. Kobayashi, S. Kawano, M. Yamanaka, and S. Kawata, "High-resolution confocal microscopy by saturated excitation of fluorescence," Phys. Rev. Lett. **99**, 228105 (2007).
8. T. Dertinger, R. Colyer, G. Iyer, S. Weiss, and J. Enderlein, "Fast, background-free, 3D super-resolution optical fluctuation imaging (SOFI)," P. Natl. Acad. Sci. USA **106**(52), 22287–22292 (2009).
9. J. Yao, L. Wang, C. Li, C. Zhang, and L. V. Wang, "Photoimprint photoacoustic microscopy for three-dimensional label-free subdiffraction imaging," Phys. Rev. Lett. **112**, 014302 (2014).
10. J. Miyazaki, H. Tsurui, A. Hayashi-Takagi, H. Kasai, and T. Kobayashi, "Sub-diffraction resolution pump-probe microscopy with shot-noise limited sensitivity using laser diodes," Opt. Express **22**(8), 9024–9032 (2014).
11. C. F. Kuang, S. Li, W. Liu, X. Hao, Z. T. Gu, Y. F. Wang, J. H. Ge, H. F. Li, and X. Liu, "Breaking the diffraction barrier using fluorescence emission difference microscopy," Sci. Rep. **3**(1441) (2013).
12. H. Dehez, M. Piche, and Y. D. Koninck, "Resolution and contrast enhancement in laser scanning microscopy using dark beam imaging," Opt. Express **21**(13), 15912–15925 (2013).
13. S. Segawa, Y. Kozawa, and S. Sato, "Resolution enhancement of confocal microscopy by subtraction method with vector beams," Opt. Lett. **39**(11), 3118–3121 (2014).

#238174 - $15.00 USD Received 16 Apr 2015; revised 11 May 2015; accepted 12 May 2015; published 15 May 2015

14. N. Wang, J. Miyazaki, J. He, K. Seto, and T. Kobayashi, "Sub-diffraction-limit imaging using mode multiplexing," Opt. Commun. **343**, 28–33 (2015).
15. S. Segawa, Y. Kozawa, and S. Sato, "Demonstration of subtraction imaging in confocal microscopy with vector beams," Opt. Lett. **39**(15), 4529–4532 (2014).
16. S. You, C. Kuang, Z. Rong, and X. Liu, "Eliminating deformations in fluorescence emission difference microscopy," Opt. Express **22**(21), 26375–26385 (2014).
17. N. Wang and T. Kobayashi, "Numerical study of the subtraction threshold for fluorescence difference microscopy," Opt. Express **22**(23), 28819–28830 (2014).
18. X. Hao, C. Kuang, T. Wang, and X. Liu, "Effects of polarization on the de-excitation dark focal spot in STED microscopy," J. Opt. **12**, 115707 (2010).
19. C. Yuan, G. Situ, G. Pedrini, J. Ma, and W. Osten, "Resolution improvement in digital holography by angular and polarization multiplexing," Appl. Opt. **50**(7), B6–B11 (2011).
20. S. Galiani, B. Harke, G. Vicidomini, G. Lignani, F. Benfenati, A. Diaspro, and P. Bianchini, "Strategies to maximize the performance of a STED microscope," Opt. Express **20**(7), 7362–7374 (2012).
21. Y. Chen, H. Lin, M. J. Ludford-Menting, A. H. Clayton, M. Gu, and S. M. Russell, "Polarization of excitation light influences molecule counting in single-molecule localization microscopy," Histochem. Cell Biol. **143**(1), 11–19 (2015).
22. N. Wang and T. Kobayashi, "Numerical calibration of the spatial overlap for subtraction microscopy," Opt. Express accepted.
23. B. Richards and E. Wolf, "Electromagnetic diffraction in optical systems. II. structure of the image field in an aplanatic system," Proc. R. Soc. Lond. A **253**, 358–379 (1959).
24. D. Ganic, X. Gan, and M. Gu, "Focusing of doughnut laser beams by a high numerical-aperture objective in free space," Opt. Express **11**(21), 2747–2752 (2003).
25. G. M. Lerman and U. Levy, "Effect of radial polarization and apodization on spot size under tight focusing conditions," Opt. Express **16**(7), 4567–4581 (2008).
26. R. C. Jones, "A new calculus for the treatment of optical systems," J. Opt. Soc. Am. **31**(7), 488–493 (1941).
27. W. H. Mcmaster, "Matrix representation of polarization," Rev. Mod. Phys. **33**(1), 8–28 (1961).
28. M. Stalder and M. Schadt, "Linearly polarized light with axial symmetry generated by liquid-crystal polarization converters," Opt. Lett. **21**(23), 1948–1950 (1996).

1. Introduction

Various types of superresolution techniques have achieved great success in improving the resolving power of optical far-field microscopes during last twenty years, such as stimulated emission depletion (STED) microscopy [1], structured illumination microscopy (SIM) [2], photoactive localization microscopy (PALM) [3], stochastic optical reconstruction microscopy (STORM) [4], and others [5–10]. Recently, mathematically calibrated microscopes, such as fluorescence emission difference (FED) microscopy [11], scanning laser mode microscopy (SLAM) [12], and others [13, 14], have attracted interests for being able to provide a simple approach to break the diffraction barrier. The concept is to subtract two fluorescence images captured by two excitation lasers with the same wavelength but with different spatial intensity distributions, e.g., solid and donut shapes. Because the quality of subtracted images strongly depends on the spot shapes of the two excitation lasers and the implemented subtraction factors, the possible problems of nonlinearities and over-process resulting from the subtraction could be generated. To reduce the distortion and negative sidebands brought by improper illumination, excitation beams with radial and azimuthal polarizations and with extended solid and hollow spot shapes have been proposed [15, 16]. Further to achieve appropriate subtraction, concept of subtraction threshold has also been constructed [17]. However, the imaging quality can be easily deteriorated by imperfect polarizations in coherent optical microscopes [18–21]. Especially for fluorescence subtraction microscopy, the resolution enhancement is obtained from direct subtraction of fluorescence images, in which the quality of the polarization for excitation should be considered significantly. However, there has been no report on the detailed study of the effects of the imperfect polarization on the subtracted parameters in such microscopes until now. In this paper, a numerical model is built based on the vector beam diffraction theory (VBDT) and it is applied to investigate the importance of the polarizations in fluorescence difference

#238174 - $15.00 USD Received 16 Apr 2015; revised 11 May 2015; accepted 12 May 2015; published 15 May 2015

microscopy. The resolution, peak intensity, and further parameters in subtracted images are quantitatively evaluated by altering the polarization described by the Jones matrices. It is found that when the wave plate for polarization conversion deviates from normal incidence by 10°, the resolution deterioration is about 5%; peak intensity decreases within 3%; the corresponding amplitude of negative sidebands is reduced by about 5%. The deviation from appropriate polarization conditions lead to easier over-subtraction and the threshold peak intensity decreases for sample sizes of smaller than 0.1λ. The subtraction factor of 0.6 is found to be able to eliminate the spot deformation after subtraction caused by the deviation of the polarizations. Simulation results with a combined radially and azimuthally polarized spots for excitation are also given.

2. Principle and numerical models

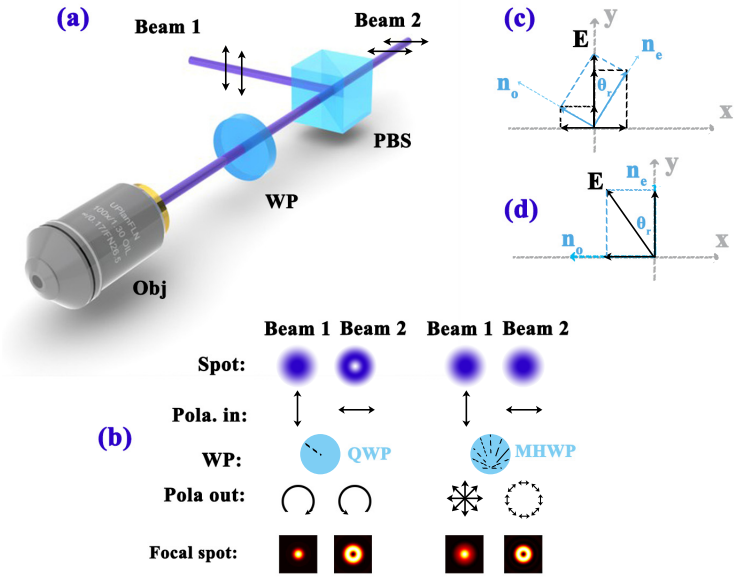

Fig. 1. (a) Schematic of polarization conversion for excitation beams in subtraction microscopy. (b) Two groups of polarization combinations for excitation. (c) Electric field components with rotated wave plate. (d) Electric field components with fixed wave plate. PBS: polarization beam splitter; WP: wave plate; Obj: objective lens; QWP: quarter wave plate; MHWP: mosaic half wave plate.

The schematic of polarization conversion in the subtraction microscope is depicted in Fig. 1(a). To avoid the interference between each other, two orthogonally linear-polarized excitation beams are combined with a polarization beam splitter and converted into desired polarization combinations with corresponding wave plates. Two combinations of spots and polarizations are usually used for excitation, as are shown in Fig. 1(b). The first group is the combination of a solid-shape spot and a donut-shape spot generated with a vortex phase plate. Then they are converted into right-handed and left-handed circular polarization after passing through a quarter-wave plate (QWP). The second group is the combination of radially and azimuthally polarized spots converted from two solid-shape spots using a mosaic half wave plate (MHWP). With each of the polarization combinations, the solid and donut focal spots for excitation can be obtained.

#238174 - $15.00 USD Received 16 Apr 2015; revised 11 May 2015; accepted 12 May 2015; published 15 May 2015

The mathematical formula of subtracted image can be expressed as [17, 22]:

$$I_{RAW}(x,y,z,\theta_r,r,\gamma) = I_S(x,y,z,\theta_r) * Ob(x,y,r) - \gamma \cdot I_D(x,y,z,\theta_r) * Ob(x,y,r)$$

$$I(x,y,z,\theta_r,r,\gamma) = \begin{cases} I_{RAW}(x,y,z,\theta_r,r,\gamma) & I_{RAW}(x,y,z,\theta_r,r,\gamma) \geq 0 \\ 0 & I_{RAW}(x,y,z,\theta_r,r,\gamma) < 0 \end{cases} \quad (1)$$

where γ is the subtraction factor, $*$ is the convolution, I_S and I_D are the focused solid and donut spots, the point spread functions (PSFs) of which can be derived from VBDT [23–25]. *Ob* is the sample. They are expressed as:

$$E_{x,y,z}(x,y,z,\theta_r) = \frac{iC}{\lambda}\int_0^{2\pi}\int_0^{\arcsin(NA/n)} A_{AMP}\cdot A_{Phase}\cdot A_L \begin{bmatrix} P_x(\theta_r) \\ P_y(\theta_r) \\ P_z(\theta_r) \end{bmatrix} \sin\theta \cdot e^{-ik\{z\cos\theta+\sqrt{x^2+y^2}\sin\theta\cos[\varphi-\arctan(y/x)]\}} d\theta d\varphi \quad (2)$$

$$I_{S,D}(x,y,z,\theta_r) = |E_x|^2 + |E_y|^2 + |E_z|^2 \quad (3)$$

$$Ob(x,y,r) = C_0 e^{-(4\ln 2)\frac{x^2+y^2}{r^2}} \quad (4)$$

Here C and C_0 are the normalization constants; λ is the wavelength of incident light; *NA* is the numerical aperture of the objective lens; n is the refractive index of the contact medium between the objective and the cover glass of the sample, the value of which is 1.518 for the immersion oil; k is the wave number; A_{AMP} is the amplitude factor; A_{PHASE} is the phase factor; r is the preset full width at half maximum (FWHM) of the sample envelope. The $A_{AMP} = 1$ means the plane wave is used to simulate the intensity distribution of the incident excitation lasers; the $A_{PHASE} = e^{i\varphi}$ is the phase distribution of the vortex phase plate. The set values of A_{AMP} and A_{PHASE} for I_S and I_D are shown in Table 1.

Table 1. Parameter sets for I_S and I_D.

	Group 1			Group 2		
I_{PSF}	Polarization	A_{AMP}	A_{PHASE}	Polarization	A_{AMP}	A_{PHASE}
I_S	Right Circular	1	1	Radial	1	1
I_D	Left Circular	1	$e^{i\varphi}$	Azimuthal	1	1

A_L is the vector weight matrix of the aplanatic objective lens, calculated as follows:

$$A_L = \sqrt{\cos\theta}\begin{bmatrix} 1+(\cos\theta-1)\cos^2\varphi & (\cos\theta-1)\cos\varphi\sin\varphi & -\sin\theta\cos\varphi \\ (\cos\theta-1)\cos\varphi\sin\varphi & 1+(\cos\theta-1)\sin^2\varphi & -\sin\theta\sin\varphi \\ \sin\theta\cos\varphi & \sin\theta\sin\varphi & \cos\theta \end{bmatrix} \quad (5)$$

$[Px, Py, Pz]$ is the unit vector matrix of the polarization. According to the Jones Calculus [26, 27],the electric field of s- or p-polarized light has components along the tilted crystal axis and then they are projected to the horizontal and vertical axes when rotating the wave plate. The phase delay between the two birefringent optical axes is $\delta = kd(n_o - n_e)$, where d is the thickness of wave plate; n_o and n_e are the refractive indices of ordinary and extraordinary optical axes, respectively. For a QWP of negative crystal, δ is $\pi/2$. From Fig. 1(c), Jones matrices of the horizontal and vertical electric field components for s- and p-polarized beams after a negative-type QWP can be written as:

$$s-p:\begin{bmatrix} P_x \\ P_y \\ P_z \end{bmatrix} = \begin{bmatrix} (1-i)\sin\theta_r\cos\theta_r \\ \cos^2\theta_r + i\sin^2\theta_r \\ 0 \end{bmatrix}, p-p:\begin{bmatrix} P_x \\ P_y \\ P_z \end{bmatrix} = \begin{bmatrix} \sin^2\theta_r + i\cos^2\theta_r \\ (1-i)\sin\theta_r\cos\theta_r \\ 0 \end{bmatrix} \quad (6)$$

#238174 - $15.00 USD Received 16 Apr 2015; revised 11 May 2015; accepted 12 May 2015; published 15 May 2015

where θ_r is the angle between the electric field of s-polarized beam and the fast axis. Then the intensity distributions of focused spots with different angles of the QWP can be calculated. Because the long and short axes of the focused spots are always along the fast and slow axes of the wave plates, it is inconvenient to analyzing the resolutions along two perpendicular axes when the focused spots are tilted. Fixing the wave plate and rotating the polarization can be a calculation strategy to solve this problem. Then the long and short axes of the focused spots can be fixed to the horizontal or vertical axes. As is shown in Fig. 1(d), the Jones matrices used to calculate the sectioning lines can be written as:

$$s-p:\begin{bmatrix} P_x \\ P_y \\ P_z \end{bmatrix}=\begin{bmatrix} -i\sin\theta_r \\ \cos\theta_r \\ 0 \end{bmatrix}, p-p:\begin{bmatrix} P_x \\ P_y \\ P_z \end{bmatrix}=\begin{bmatrix} \cos\theta_r \\ -i\sin\theta_r \\ 0 \end{bmatrix} \tag{7}$$

For the radially or azimuthally polarized beams generated from MHWP, the Jones matrices are [28]:

$$s-p:\begin{bmatrix} P_x \\ P_y \\ P_z \end{bmatrix}=\begin{bmatrix} \cos(\varphi-\theta_r) \\ \sin(\varphi-\theta_r) \\ 0 \end{bmatrix}, p-p:\begin{bmatrix} P_x \\ P_y \\ P_z \end{bmatrix}=\begin{bmatrix} \sin(\varphi-\theta_r) \\ -\cos(\varphi-\theta_r) \\ 0 \end{bmatrix} \tag{8}$$

where φ is the azimuthal angle. Then the focal PSFs and subtracted spots related with the angles θ_r for different polarizations can be obtained. In order to quantitatively analyze the quality of the image, the peak intensity and amplitude of negative sidebands after subtraction are defined as:

$$I_{peak}=\frac{MAX[I(x,y,z,\theta_r,r,\gamma)]}{MAX[I(x,y,z,\theta_r,r,0)]} \tag{9}$$

$$|I_{Neg}|=\begin{cases} 0 & MIN[I_{RAW}(x,y,z,\theta_r,r,\gamma)]\geq 0 \\ \frac{|MIN[I_{RAW}(x,y,z,\theta_r,r,\gamma)]|}{MAX[I(x,y,z,\theta_r,r,\gamma)]} & MIN[I_{RAW}(x,y,z,\theta_r,r,\gamma)]<0 \end{cases} \tag{10}$$

The subtraction threshold condition, which describe the appropriate subtraction [17], and normalized peak intensity at threshold under the condition, are expressed by Eqs. (11) and (12), respectively.

$$FWHM_{Ob(x,y,r_0)}=FWHM_{I(x,y,z,\theta_r,r_0,\gamma_0)} \tag{11}$$

$$I_P=\frac{MAX[I(x,y,z,\theta_r,r_0,\gamma_0)]}{MAX[I(x,y,z,\theta_r,r_0,0)]} \tag{12}$$

Then the effects of the polarization on the FWHM resolution, ellipticity, peak intensity, negative sidebands, subtraction threshold and peak intensity after subtraction can be carried out.

3. Simulation results

3.1. Linear and circular polarizations.

The calculated fluorescence and subtracted spots with polarizations of different circularity are shown in Fig. 2. The preset sample size is $r=0.1\lambda$. From Fig. 2(a), it can be seen that the shape of the focused spot varies with different polarization status. The focused solid spot has elliptical shape when the incident light is linearly or elliptically polarized. Because of the phase distribution, the center of the donut spot is round and has zero intensity only if θ_r is -45°, where the polarization is left-handed circular. This is the appropriate angle for illumination in subtraction microscope. As is shown in Fig. 2(b), the subtracted images with $\theta_r=-45^\circ$ keep the same circularity while images with this angle $\pm 10^\circ$ have varying circularities after subtraction. Figures 2(c)–2(e) display the FWHM values of the cross sectioning profiles along

#238174 - $15.00 USD Received 16 Apr 2015; revised 11 May 2015; accepted 12 May 2015; published 15 May 2015

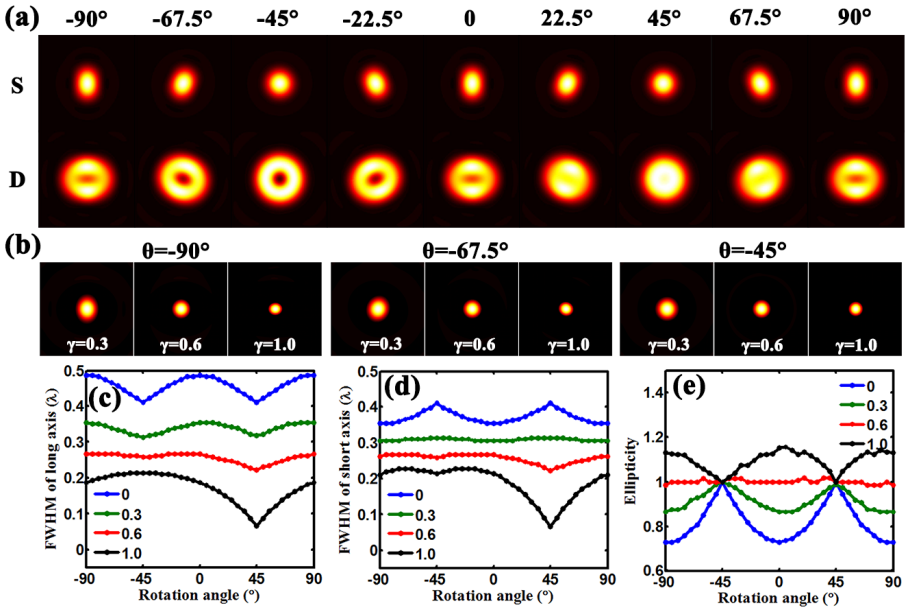

Fig. 2. (a) Convoluted solid and donut fluorescence images with different rotation angles of the QWP. The sample has size of $r = 0.1\lambda$. (b) Subtracted images with factors of γ=0.3, 0.6, 1.0 for $\theta_r = -90^\circ$, -67.5°, -45°. (c)–(e) FWHM values of sectioning profiles along the long and short axes, and ellipticity with different subtraction factors of γ=0, 0.3, 0.6, 1.0 versus different rotation angles (θ_r).

the long and short axes of subtracted focal spots and corresponding ellipticities with factors of γ=0, 0.3, 0.6, 1.0. It can be seen that, the FWHM values of subtracted spots are fluctuating by about 0.1λ when rotating the QWP by π; the FWHM values change within 5% even when the angles of the QWP deviate from the right angle for 10°; the ellipticities of the spots after subtraction with the two critical angles of -45° and 45° are both unity; with subtraction factors of larger than 0.6, the long and short axes of the subtracted spots are reversed. The ellipticity here is defined as the ratio of FWHM values on the primary short and long axes of the focused spot. What is more, it is interesting to find that the factor of 0.6 can almost eliminate the errors of ellipticity induced by the misalignments of the polarization. It also indicates that when the factor of 0.6 is implemented in the subtraction scheme, the problem of polarization aberration cannot be intuitively found out from the subtracted images.

The evolution of peak intensity, amplitude of negative sidebands and the subtraction threshold are shown in Fig. 3. From Fig. 3(a), it can be seen that the subtracted peak intensities are maximal when $\theta_r = -45^\circ$ even with different subtraction factors. With $\theta_r = 45^\circ$, the center of donut spot is not completely dark, so the peak intensity drops significantly after the convolution with samples and the following subtraction. The Fig. 3(b) describes that the decreased amount of peak intensity after subtraction is about 2.5% if the angle of QWP is displaced with 10° and subtraction factor of 1. Thus, the problem of signal loss due to the imperfect polarization for excitation within 10° is not serious. Besides, the negative sidebands are generated inevitably after subtraction. However, from Fig. 3(c), the values of negative sidebands introduced are similar in a wide range from -90° to 0°. The deviation of the polarization may reduce the negative sidebands by 5% as is shown in Fig. 3(d). It describes that the amplitude of negative sidebands after subtraction is insensitive to the ellipticity of the polarization, either. Similarly, the calcula-

#238174 - $15.00 USD Received 16 Apr 2015; revised 11 May 2015; accepted 12 May 2015; published 15 May 2015

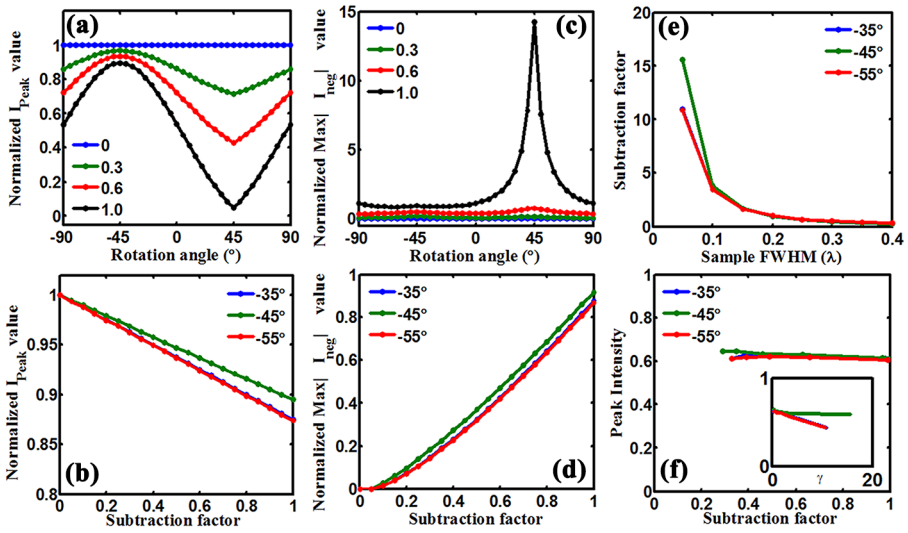

Fig. 3. (a) Peak intensity and (c) Negative sidebands versus rotation angles of QWP with subtraction factors of γ=0, 0.3, 0.6, 1.0. (b) Peak intensity and (d) Negative sidebands versus subtraction factors with rotation angles of $\theta_r = -35^\circ, -45^\circ, -55^\circ$. (e) Subtraction threshold line. (f) Threshold peak intensity curves.

tions on the resolution, peak intensity and negative sidebands with different sample sizes have been carried out. The curves give the similar evolutions as present ones which will not be illustrated in further details. For a sample size of 0.4λ, the variation of FWHM values of subtracted spots is by about 0.1λ versus the rotation angles of the QWP. The peak intensities or negative sidebands are affected by less than 1% with 10° deviation from the right angle. The subtraction threshold lines are shown in Fig. 3(e). It can be seen that the threshold subtraction factors for $\theta_r = -45^\circ$ are a little larger than the cases of -35° and -55° with sample sizes of smaller than 0.1λ. It means the polarization-deviated excitation is vulnerable for over-subtraction and it mainly acts on the fine structures in the sample. Meanwhile, from the Fig. 3(f), it can be seen that the threshold peak intensity factors slightly drop when increasing the subtraction factors. It means that the deviation of polarization will not introduce significant signal loss at the subtraction threshold for sample sizes larger than 0.1λ.

3.2. Radial and azimuthal polarizations.

The calculation results with radially and azimuthally polarized excitation spots are shown in Fig. 4. The focused PSFs with different rotation angles of MHWP are shown in Fig. 4(a). Because the evolutions of the subtracted spot shapes are periodical appearing, only the angles between -45° and 45° are analyzed here. From Fig. 4(b), it can be seen that the subtracted spot shapes are not deformed with displaced polarization angles while the resolutions are a little worse than the case of 0° for MHWP. Figures 4(c)–4(e) depict the FWHM values, peak intensities, and the values of negative sidebands when changing the angles of the MHWP. It can be found that when the angle of MHWP is 0° and subtraction factor keeps the same, the resolved FWHM values are smaller than them with other angles. Meanwhile, the peak intensity is also maximal at the angle of 0°. It is possible to use these two parameters to calibrate the angles of the used MHWP. When rotating the plate, the angle with maximal peak intensity and minimal FWHM values correspond to the appropriate angle for MHWP in subtraction microscope scheme. The amplitude of negative sidebands is insensitive to the rotation angles

#238174 - $15.00 USD Received 16 Apr 2015; revised 11 May 2015; accepted 12 May 2015; published 15 May 2015

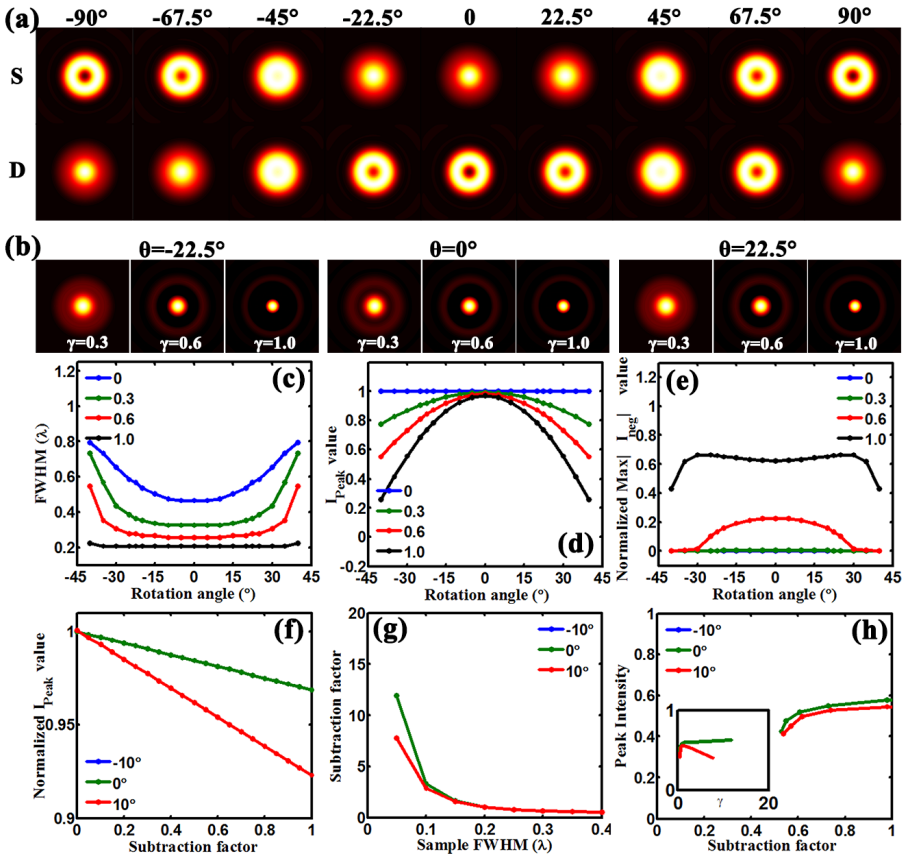

Fig. 4. Simulation results with radial and azimuthal polarization. (a) Excitation spots versus different angles of wave plate. (b) Subtracted images with factors of 0.3, 0.6 and 1.0 for the rotation angles of -22.5°, 0°, 22.5°.

of the plate, as is shown in Fig. 4(e). From Fig. 4(f), it can be seen that the peak intensity decrease is about 5% when the angle is deviated with 10° and subtraction factor of 1. The subtraction threshold lines and the threshold peak intensity lines are shown in Figs. 4(g) and 4(h), respectively. Similar to the results in the case of circular polarization, the threshold lines show that the right angle of 0° can stand the over-subtraction than the incorrect polarizations. Meanwhile, the threshold peak intensity factors are a little smaller for the displaced angles. It means that when get the appropriate subtraction, the peak intensity is slightly decreased, especially for the sample sizes of smaller than 0.1λ.

4. Conclusion.

In summary, we have built a numerical model to evaluate the effects of polarization for subtraction microscope based on the vector beam diffraction theory. By modulating the Jones matrices, the effects of different polarization status on the parameters of resolution, ellipticity, peak intensity, negative sidebands and subtraction threshold in fluorescence emission difference microscopy are quantitatively investigated. The resolution deterioration, signal loss and intensity reduction of negative sidebands are all within 5% for both of the polarization combinations for excitation even that the angles of wave plates are deviating from the normal incidence by 10°.

#238174 - $15.00 USD Received 16 Apr 2015; revised 11 May 2015; accepted 12 May 2015; published 15 May 2015

The corresponding threshold peak intensity curve finds that the signal loss at appropriate subtraction is negligibly small for sample sizes of larger than 0.1λ. The rotating angle of polarizer being 45° must be critically avoided, since it can generate serious signal intensity loss and resolution deterioration. The subtraction factor of 0.6 is found to be a specially behaving parameter for the case when the polarization is modified with a quarter wave plate. With this factor, the ellipticity is always unity even the excitation beams are linearly or elliptically polarized. To calibrate the polarization, ellipticity variation, or peak intensity after subtraction can be used. Furthermore, the simulation here is carried out based on the model in ideal conditions. However, calculations in this paper can basically describe and evaluate the effects of polarization on the parameters for fluorescence subtraction microscopy even though the confocal detection parameter or noise effect is not included in the model. The improved model including them is to be presented in future work. Sensitive fluorescence detection with high signal to noise ratio is necessary for experimental demonstration of present calculation. Our related experiments are in progress.

#238174 - $15.00 USD Received 16 Apr 2015; revised 11 May 2015; accepted 12 May 2015; published 15 May 2015